

Adaptive Sampling for Fast and Accurate Metamodel-Based Sensitivity Analysis of Complex Electromagnetic Problems

*Original*

Adaptive Sampling for Fast and Accurate Metamodel-Based Sensitivity Analysis of Complex Electromagnetic Problems / Lagouanelle, P; Freschi, F; Pichon, L. - In: IEEE TRANSACTIONS ON ELECTROMAGNETIC COMPATIBILITY. - ISSN 0018-9375. - STAMPA. - 65:6(2023), pp. 1820-1828. [10.1109/TEMC.2023.3320285]

*Availability:*

This version is available at: 11583/2984800 since: 2024-01-02T14:09:49Z

*Publisher:*

IEEE

*Published*

DOI:10.1109/TEMC.2023.3320285

*Terms of use:*

This article is made available under terms and conditions as specified in the corresponding bibliographic description in the repository

*Publisher copyright*

(Article begins on next page)

# Adaptive Sampling for Fast and Accurate Metamodel-Based Sensitivity Analysis of Complex Electromagnetic Problems

Paul Lagouanelle , Fabio Freschi , and Lionel Pichon 

**Abstract**—This article presents the development of an adaptive sampling strategy for building surrogate models of complex electromagnetic systems. Accurate sensitivity analysis is crucial to electromagnetic compatibility but usually requires a few thousand calls of the numerical model if performed using classical Monte Carlo sampling. In the case of an expensive computational model, this results in extremely long computation. Hence, with only a few calls of the numerical model, surrogate models are built to approximate the behavior of the system. This accurate predictor can then be used instead of the expensive computational model for various analyses. The active learning sampling strategy has been tested successfully on a realistic finite-element method model.

**Index Terms**—Approximation methods, metamodeling, numerical models, sensitivity analysis (SA).

## I. INTRODUCTION

**S**ENSITIVITY analysis (SA) can be used on both numerical models and experimental prototypes in order to predict and quantify the variations of an output of interest regarding defined variations of input parameters, thus helping in the design of new systems and the improvement of existing devices. Owing to the recent growth of electrical engineering for both domestic and industrial applications, the need of fast and accurate SA for such complex systems has been constantly increasing in the case of electromagnetic compatibility (EMC) engineering.

Because of the overall complexity of most current numerical models, computation time is increasing rapidly for SA when the variation of several input parameters at once is considered. A possible work-around is to use surrogate modeling (or metamodeling), which builds a predictor of the model using a given

training dataset. This metamodel is an analytical function that can be computed fast a great number of times. It can be used in lieu of the existing simulation model (or experimental model). Thus, the global SA, like Sobol' indices [1] computed with Monte Carlo (MC) methods, is performed on the predictor at a low computation cost easily.

Thanks to their flexibility, ease of implementation, great efficiency with stochastic models, high accuracy for high-order interaction, and nonlinearities, metamodels enable fast and easy computation of global sensitivity indices on complex numerical models [2], provided that an accurate metamodel has been built. Regarding EMC problems in general, many numerical methods have been recently developed in order to reduce the numerical cost of SA. In [3], both response surface methodology (RSM) and polynomial chaos expansion (PCE) are used to perform accurate SA of crosstalks among differential vias. Both the methods have been successfully validated using simulation data. In [4], PCE has been used successfully to construct a surrogate model of the radiated field in shielded wires. Surrogate models can also be used for optimization in EMC design, as in [5], where an RSM-based optimization process is used to efficiently design multilayered shields.

The goal of the work presented here is to reduce the number of samples needed for the surrogate model setup, thus reducing the number of calls of the heavy computational model. In [6], a performance-driven model is fully developed and validated for the design of antenna structures. Koziel and Pietrenko-Dabrowska [6] managed to reduce the number of calls of the electromagnetic (EM) model by 60% (on average) compared to a classical analysis. In [7], the use of Smolyak's sparse grid algorithm is presented for uncertainty quantification for EM systems. As in [7], most of these numerical methods can be enhanced using adaptive sampling to greatly reduce the initial samples for the metamodel setup [8]. In [9], a radiated immunity test is studied with a Thévenin-based metamodel paired with simple adaptive sampling, which manages to reduce the computation time from  $\sim 119$  h using a finite-element method (FEM) solver to only 19 s. For complex EMC problems, adaptive sampling has notably been used with Kriging metamodeling of radiated susceptibility in coaxial shielded cables [10]. But also to perform global SA of an EM interference filter [11].

Therefore, this work focuses on the design of an adaptive sampling strategy for metamodeling. First, this article presents

Manuscript received 30 April 2023; revised 15 September 2023; accepted 26 September 2023. Date of publication 12 October 2023; date of current version 13 December 2023. (Corresponding author: Fabio Freschi.)

Paul Lagouanelle is with the Dipartimento Energia "G. Ferraris," Politecnico di Torino, 10129 Torino, Italy, and also with the Group of Electrical Engineering Paris, UMR CNRS 8507, CentraleSupélec, Université Paris-Saclay Sorbonne Université, 91192 Gif-sur-Yvette, France (e-mail: paul.lagouanelle@latmos.ipsl.fr).

Fabio Freschi is with the Dipartimento Energia "G. Ferraris," Politecnico di Torino, 10129 Torino, Italy (e-mail: fabio.freschi@polito.it).

Lionel Pichon is with the Group of Electrical Engineering Paris, UMR CNRS 8507, CentraleSupélec, Université Paris-Saclay Sorbonne Université, 91192 Gif-sur-Yvette, France (e-mail: lionel.pichon@centralesupelec.fr).

Color versions of one or more figures in this article are available at <https://doi.org/10.1109/TEMC.2023.3320285>.

Digital Object Identifier 10.1109/TEMC.2023.3320285

the development and the design parameters required for an adaptive strategy for polynomial-chaos-based Kriging (PCK) metamodeling. Then, based on various test functions and several sampling strategies, a partition design is selected to greatly reduce the number of calls of the input computational model. The core of the work lies in the careful selection of the refinement design, where the parameter space is subdivided based on a local nonintrusive cross-validation (CV) criterion. Unlike other existing adaptive strategies, the global consistency of the metamodel is achieved by ensuring a local consistency of every surrogate model built in every partition of the parameter space. Finally, the resulting algorithm is tried on a realistic wireless power transfer (WPT) system FEM model, on which accurate SA is crucial for EMC studies.

## II. SURROGATE MODELING ALGORITHM

### A. Surrogate Model

This work focuses on two surrogate models, PCE and Kriging, along with their combination PCK, which have been proven quite efficient for building accurate predictors and performing various global SAs on a wide range of complex models, for example, in the case of EM device optimization [12], where Kriging has been proven better compared to other surrogate processes. PCE has been proven successful at approximating magnetic flux density at a lower computation cost than regular simulations [13]. As for PCK metamodeling, it has been recently used in the case of computational dosimetry for estimating specific absorption rate values [14].

The surrogate model used here is an exact interpolator: PCK metamodeling combines both PCE and Kriging to predict the variations of a given model  $\mathcal{M}(X)$ . Kriging is used to interpolate the local variations of the output model, while PCE is useful for global approximation. A PCK metamodel is defined as [15]

$$\widehat{\mathcal{M}}(X) = \sum_{\alpha \in \mathcal{A}} y_{\alpha} \psi_{\alpha}(X) + \sigma^2 Z(X, \omega) \quad (1)$$

where  $\sum_{\alpha \in \mathcal{A}} y_{\alpha} \psi_{\alpha}(X)$  is a weighted sum of orthonormal polynomials describing the trend of the PCK model and  $\sigma^2 Z(X, \omega)$  is a zero-mean stationary Gaussian process with a variance of  $\sigma^2$ . PCK can be interpreted as a Kriging metamodel with a polynomial trend, whose characteristics are unknown. Therefore, the PCK metamodel is built in two parts: the computation of the polynomial coefficients ( $y_{\alpha}$ ) on one side and the Kriging hyperparameters on the other side. The computation of these metamodel parameters is performed by the UQLab framework available on MATLAB [16].

Let us consider a set  $\{(X_1, Y_1), \dots, (X_N, Y_N)\}$  of  $N$  input samples. Using this set, one can build a PCK metamodel  $\widehat{\mathcal{M}}$ . The consistency of the metamodel is evaluated by the leave-one-out error (LOO):

$$LOO = \frac{1}{N} \sum_{i=1}^N \left( \frac{\|\widehat{\mathcal{M}}_{/i}(X_i) - Y_i\|}{\|Y_i\|} \right)^2 \quad (2)$$

where  $\widehat{\mathcal{M}}_{/i}$  is the mean predictor that was trained using all  $(X, Y)$  but  $(X_i, Y_i)$ . The LOO enables us to evaluate the consistency of the metamodel considering its build. If the LOO is close to 1, the metamodel is highly modified if one datapoint is taken out of the training dataset, whereas the smallest it is, the least it will be modified.

### B. Variance-Based SA

In order to perform global SA using metamodels, the well-known Sobol' indices [1] have been chosen as our sensitivity trackers. The first-order Sobol index for a parameter  $P$  is a simple quantity varying from 0 (almost independent) to 1 (the more dependent) quantifying the dependence of the output model on a given parameter  $P$  regarding a variation of several parameters simultaneously. When using PCE-based metamodels, the computation of the Sobol' indices can be easily extracted from the polynomial decomposition [see (1)].

Let us consider a model output  $\mathbf{Y} = \mathcal{M}(\mathbf{X})$  with  $d$  input parameters  $(P_1, \dots, P_d)$ . Thanks to the uniqueness of Sobol' decomposition, the output variance  $\text{Var}(\mathbf{Y})$  can be expressed as

$$\begin{aligned} \text{Var}(\mathbf{Y}) &= \sum_{s=1}^d \sum_{i_1 < \dots < i_s} V_{i_1, \dots, i_s} \\ \text{Var}(\mathbf{Y}) &= \sum_{i=1}^d V_i + \sum_{(i,j), i < j} V_{ij} + \dots + V_{12\dots d} \end{aligned} \quad (3)$$

with the following definitions for the partial variance terms:

$$\begin{aligned} V_i &= \text{Var}_{P_i}(\mathbb{E}_{\mathbf{X}_{/i}}(\mathbf{Y}|P_i)) \\ V_{ij} &= \text{Var}_{P_i P_j}(\mathbb{E}_{\mathbf{X}_{/ij}}(\mathbf{Y}|P_i, P_j)) \\ V_{i_1, \dots, i_s} &= \text{Var}_{P_{i_1} \dots P_{i_s}}(\mathbb{E}_{\mathbf{X}_{/i_1 \dots i_s}}(\mathbf{Y}|P_{i_1}, \dots, P_{i_s})). \end{aligned} \quad (4)$$

The variance can be decomposed in a sum of variance-based terms showing the dependence on each input individually [ $V_i$  in (3)] as well as the second-order ( $V_{ij}$ ) and higher order interactions between the various input parameters.

1) *Sobol' Indices*: Using the variance decomposition in (3), a sensitivity tracker  $S_u$  can be defined for any combination of any order of input parameters,  $\forall u = (i_1, \dots, i_s) \in \llbracket 1, d \rrbracket^s, i_1 < \dots < i_s$ :

$$S_{i_1, \dots, i_s} = \frac{V_{i_1, \dots, i_s}}{\text{Var}(\mathbf{Y})}. \quad (5)$$

The most commonly used Sobol' indices is the first-order Sobol' index,  $\forall i \in \llbracket 1, d \rrbracket$ :

$$S_i = \frac{V_i}{\text{Var}(\mathbf{Y})} = \frac{\text{Var}_{P_i}(\mathbb{E}_{\mathbf{X}_{/i}}(\mathbf{Y}|X_i))}{\text{Var}(\mathbf{Y})}. \quad (6)$$

which emphasizes the impact of the parameter  $P_i$  alone on the output model compared to other parameters. The closer it is to 1, the bigger impact it produces on the model. Higher order Sobol' indices can be interpreted in the same way; as the sensitivity of the output model is observed regarding the variations of several input parameters simultaneously, the effect of each input cannot be separated from the others. The total sum of all orders Sobol'

indices verifies

$$\sum_{i=1}^d S_i + \sum_{(i,j), i < j} S_{ij} + \dots + S_{12\dots d} = \sum_{\{u, u \subseteq [1,d]\}} S_u = 1. \quad (7)$$

2) *Total Indices*: For high-dimensional output models, the observation of all-order Sobol' indices can be difficult due to the high number of combinations. Therefore, for an input parameter  $P_i$ , a total-effect index (or total Sobol' index)  $S_i^T$  is defined by summing all the Sobol' indices using this variable, as follows:

$$S_i^T = \sum_{\{u, u \subseteq [1,d] \text{ and } i \in u\}} S_u. \quad (8)$$

Unlike  $S_i$ , where according to (7),  $\sum_{i=1}^d S_i \leq 1$ , this time the sum of all the total Sobol' indices is greater than 1, i.e.,

$$\sum_{i=1}^d S_i^T \geq 1. \quad (9)$$

Indeed, for example, for a given couple  $(P_i, P_j)$  of input parameters,  $S_{ij}$  is counted for both  $S_i^T$  and  $S_j^T$ . The equality case for inequality (9) is for an output model purely additive. The information given by  $S_i^T$  is different from the one given by  $S_i$ ; for example,  $S_i \ll 1$  does not imply necessarily  $S_i^T \ll 1$ . A total Sobol' index close to zero means that the input parameter is almost not affecting the output model, which can be useful for further simulations and experimental designs.

### C. Adaptive Sampling Strategy

Sampling strategies can be classified into two categories: static ("one-shot") sampling and sequential sampling (see [8, Fig. 1]). In static sampling, the sample size and the input dataset are chosen prior to the model evaluation. However, in our study cases, the input models are rather costly and their response is unknown. Thus, it is hard to determine an *a priori* sample, which would result in a consistent surrogate model. Hence, sequential sampling methods have been developed, where the input dataset is modified based on previous computations along the build of the metamodel.

Among sequential sampling strategies, the goal of an adaptive sampling strategy (also called active learning) is to start from a rather low number of samples and expand it in the regions of interest of the model response (red samples in Fig. 1). This results in a relatively low number of calls of the input model compared to space-filling strategies for the same level of surrogate model accuracy.

The general flowchart of an adaptive sampling strategy for surrogate modeling is displayed in Fig. 2. Given an input parameter space  $\mathcal{X}$  for an expensive computational model  $\mathcal{M}$ ,  $N$  samples are drawn from it,  $\mathbf{X} = (X_1, \dots, X_N)$ . Their corresponding model responses are computed  $\mathbf{Y} = (Y_1, \dots, Y_N)$ , and a first metamodel  $\widehat{\mathcal{M}}$  is computed using this dataset. If such a metamodel is not accurate, new samples (along with their responses) are drawn in the regions of interest, and the input dataset is enriched. The algorithm stops when the metamodel is accurate enough.

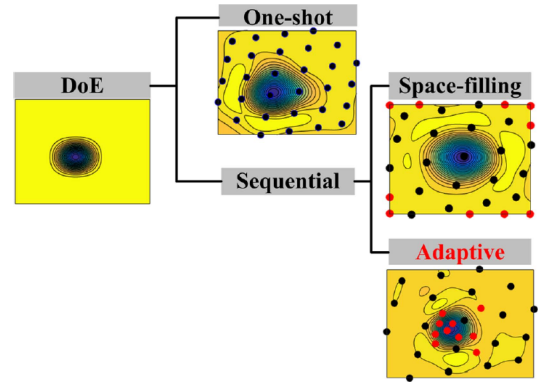


Fig. 1. Visual representation of different sampling strategies, taken from [8].

Therefore, for the design of such an active learning metamodeling process, several design parameters need to be explored: a local criterion to expand or not the dataset, a global stopping criterion, the sampling method, and finally the definition of the area of interests. The general goal is to minimize the calls of the expensive model function (blue processes in the flowchart).

### D. Design Parameters

1) *Local Criterion*: The most adaptive sampling strategy starts with a space-filling sampling method to explore the input parameter space as much as possible. Then, the expansion of the dataset in a local area is ruled by the observation of certain local metric. The metric can be model dependent (variance based, gradient based, etc.), which often leads to additional model calls and thus longer computation time in our case, or independent (usually CV errors) using only the existing dataset or the metamodel, which can be computed rapidly using the analytical predictor. Therefore, considering low input dimensionalities (no greater than ten input parameters) for the input parameter space, the aforementioned *LOO* has been considered for the local accuracy of our metamodel [see (2)]. This enables to minimize the call of the computational model.

If the local *LOO* is too high in an area, more samples are needed in this part of the input parameter space. This brings the difficult choice of defining a proper threshold for the *LOO* as a local stopping criterion (see discussion in [17]). The choice of the *LOO* as a local stopping criterion is highly motivated by its crucial use for the existing learning algorithms. Overall, the *LOO* CV error is successful at estimating the consistency of any metamodel while not being the best in every case [18]. Moreover, within a region of interest, the use of *LOO* instead of other  $k$ -fold CV error is obvious due to the low number of datapoints considered. Choosing the *LOO* as a local metric ensures that, in every area of interest considered within the input parameter space, the resulting metamodel is locally consistent. Therefore, the metamodel is globally consistent regarding the entire input parameter space.

2) *Partition Algorithm*: The choice of a CV-based adaptive sampling leads to an obvious partition design for the area of interests. The main idea is to split each inaccurate region into  $2^d$

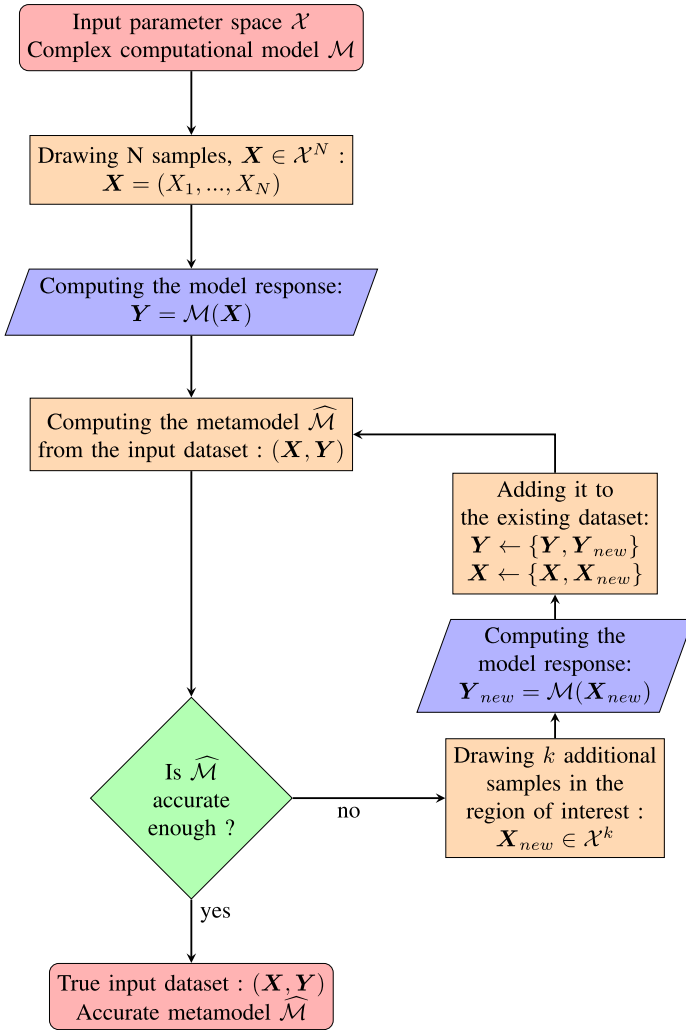


Fig. 2. Flowchart of an active learning metamodeling process, with the blue processes being the computationally expensive steps.

subregions, with  $d$  being the dimension of the input space. This quad-tree partition design [19] has already been successfully developed for solving Navier–Stokes equations in aeronautic design [20]. Although this subgridding technique is quite easy to set up, the main drawback of using it is the obvious curse of dimensionality, where the number of computed datapoints would explode for high-dimensional models. Hence, the application of this algorithm and the models studied here have responses only depending on a small number of parameters. Performing global SA prior to a complete active learning algorithm can greatly reduce the number of relevant parameters for a single analysis, thus preventing us from computing too many useless datapoints.

3) *Subdivision Limitation*: Usually, a tradeoff between the local and global criteria needs to be defined, with proper weights given to each metric in order to subdivide or not the current domain. However, in order to tackle the curse of dimensionality, which appears due to the two previous choices, an obvious choice for the global criterion is to set the maximum number of divisions allowed for partitioning to limit the total number of computations.

### III. COMPARISON OF SAMPLING METHODS

Local and global stopping criteria have been chosen with the CV *LOO* and a limit for the number of divisions, along with a partitioning subgridding technique for the generation of subspaces within area of interests where the new samples will be drawn from.

#### A. Sampling Methods Considered

Then, the goal is to determine the best way to draw samples within subdomains using either stochastic or deterministic methods. The final goal is to not compute a lot of datapoints due to the possible complexity of the considered output model; therefore, a great care should be taken in saving as many datapoints as possible when drawing samples on the various domains. The methods used for generating the initial sample and all the following subsamples have been considered identical. Thus, once a subdomain is created with partitioning, the samples are also exploring the whole subspace. Five different sampling methods have been investigated, which all have already been proven useful in the case of adaptive sampling for surrogate modeling processes among the literature [8], [21]. The following three stochastic sampling methods have been studied:

- 1) Latin hypercube sampling (LHS);
- 2) Sobol' sequence sampling (Sobol');
- 3) MC sampling;

along with the following two deterministic methods:

- 1) Halton sequence sampling (Halton);
- 2) Uniform sampling.

An example of some samples for a bidimensional parameter space is displayed in Fig. 3 after one division of the partitioning algorithm. For a  $d$ -dimensional parameter space, the number of samples in each subdomain has been set to  $2^d + 1$ . This embodies, in the case of a uniform quad-tree design, the  $2^d$  corners and the center of the subdomain. This choice has been motivated by various tests notably when comparing the decrease in the local *LOO* (higher consistency) when adding centers to the subdomains of an existing uniform partition design.

#### B. Test Functions

The algorithm with the five aforementioned sampling methods has been tested against several functions with bidimensional inputs that aim to cover a range of possible computational model outputs for EM quantities. These test functions have been chosen purely arbitrary, and this choice has only been made based on the type of output that had already been studied and the corresponding variations observed. The four bidimensional test functions are displayed in Fig. 4:

- 1) a function (a) that embodies the computation of the B-field by an infinite wire with the current  $X$  and the distance to the wire  $Y$ ;
- 2) a peak function (b) has also been chosen to represent a possible resonance where the whole bidimensional space is giving low values apart from the peak where the output is 10;
- 3) a simple square function:  $(X, Y) \rightarrow X^2 + Y^2$  (c);



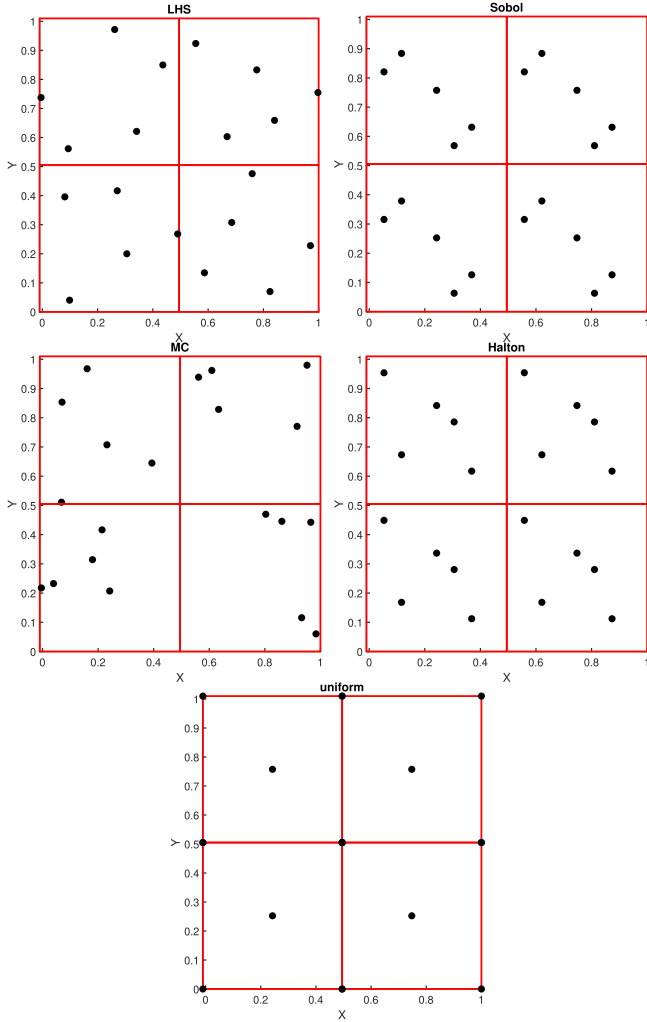


Fig. 3. Sampling methods considered: 20 calls for LHS, Sobol', MC, and Halton samplings instead of 12 calls for the uniform sampling for a bidimensional input space.

4) a bidimensional wave function (d) with a lot of local and global extrema.

C. Consistency of the Metamodels

Along testing the various sampling methods on these five functions, three different values for both the  $LOO$  threshold  $\varepsilon = [0.1, 10^{-2}, 10^{-3}]$  and the maximum number of divisions  $m = [2, 3, 4]$  have been tried. Therefore, 180 metamodels have been computed with our algorithm for all the possible combinations with five samples on each domain. In Fig. 5, a different number of samples  $n_{samples}$  against their corresponding  $LOO$  are displayed for every functions and every sampling methods studied. This number is the total number of samples required for the algorithm to converge.

The consistent metamodels for performing accurate SA will be considered only for  $LOO < 10^{-2}$ . When comparing the results for the different sampling methods, it can be seen that using local uniform sampling does not provide the best metamodels considering the  $LOO$  consistency. However, some  $LOO$  values

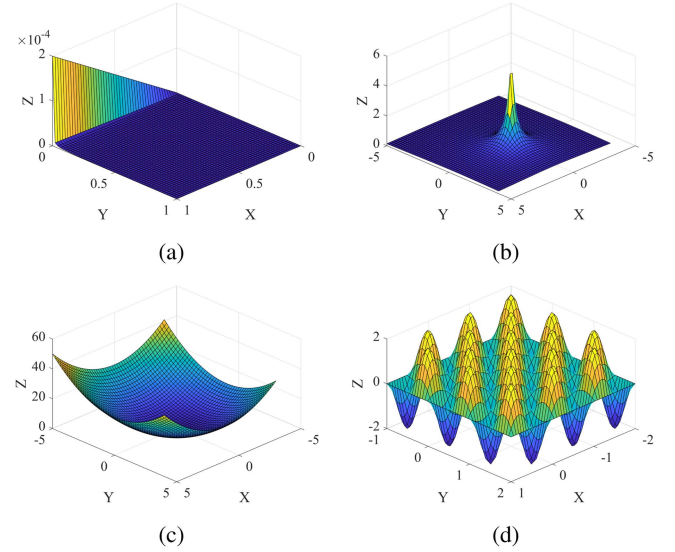


Fig. 4. (a)–(d) Test functions for comparing sampling methods on the active learning algorithm.

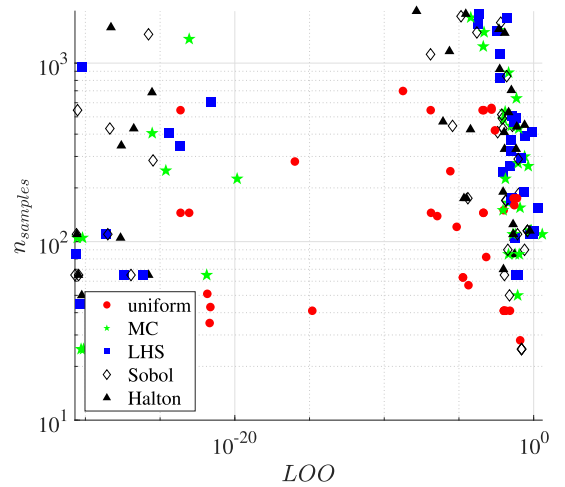


Fig. 5.  $LOO$  against  $n_{samples}$  for various test cases.

for nonuniform sampling are overly small ( $< 10^{-20}$ ), which is not needed, and some are using way too many datapoints at the same time. All in all, uniform sampling is the only one to produce consistent enough metamodels with some decent number of samples, which is already too much considering realistic computational model. Considering  $LOO$  only, uniform sampling seems to be the best compromise.

D. Validation Tests

In order to properly assess the accuracy of the predictor at estimating the real model, four MC-generated validation sets of 100 datapoints have been created (one for every test function).

Once a metamodel  $\widehat{\mathcal{M}}$  is computed with a given input dataset, a validation set  $\{(X_i, Y_i = \mathcal{M}(X_i)), \forall i \in \llbracket 1, N \rrbracket\}$  can be used

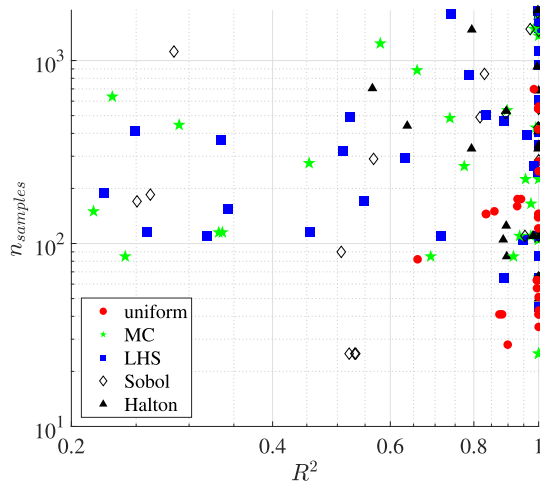


Fig. 6. Validation error  $R^2$  against  $n_{\text{samples}}$  for various test cases.

to compute a validation error for the metamodel with the well-known coefficient of determination  $R^2$ :

$$R^2 = 1 - \frac{\sum_{i=1}^N \|\widehat{\mathcal{M}}(X_i) - Y_i\|^2}{\sum_{i=1}^N \|\bar{Y} - Y_i\|^2} \quad (10)$$

where  $\bar{Y}$  is the mean value of the validation set output. The closer  $R^2$  is to 1, the better the predictor is at computing nonsampled datapoints. This coefficient is useful for comparing different metamodels on the same validation set in order to determine which one gives us the best predictor.

In Fig. 6, the validation error  $R^2$  has been displayed for the 180 computed metamodels. Among the five considered sampling methods, uniform sampling is the only one to ensure  $R^2 \sim 1$  for a fairly low number of samples. For some test cases, MC, LHS, Sobol', and Halton samplings are producing predictors with a small coefficient of determination, thus unable to accurately predict the behavior of the input model. This makes these four sampling methods highly unreliable for regular use in performing accurate SA using the active learning algorithm. Again, from this second point of view, uniform sampling is the best sampling method to balance both the number of samples and an accurate enough predictor.

### E. Discussion

If another sampling method is to be used for future computations, on these different test functions and for both analysis, Sobol' sequence sampling seems to provide the second best results. When a domain is subdivided into  $2^d$  domains, during the next loop, for the computation of the various metamodels, only  $2^d$  corners need to be added along with  $2^d$  centers as many datapoints are already available due to previous computations (see comparison in Fig. 3). This is the main interest of using uniform subgridding sampling instead of LHS or MC sampling, which would result in much more datapoints computed. Considering the quad-tree partition design with uniform sampling,

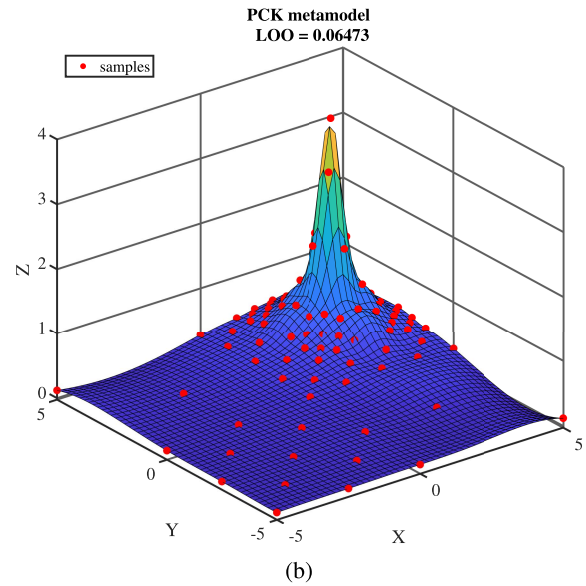
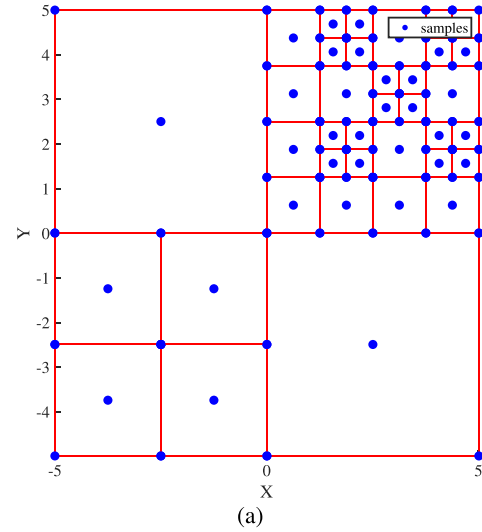


Fig. 7. Results of the active learning algorithm on a peak function [maximum at (3, 3)] for  $\varepsilon = 0.3$  and  $m = 4$ . (a) Final subdomains and samples. (b) Accurate predictor ( $n_{\text{samples}} = 97$ ,  $LOO \simeq 0.0647$ ).

the maximum number of datapoints computed is

$$n_{\text{max}} = (2^m + 1)^d + 2^{dm} \quad (11)$$

where  $d$  is the number of input parameters and  $m$  is the maximum number of divisions allowed.

An example of the final partitioning and predictor for a peak function on a bidimensional input space is shown in Fig. 7. The resulting predictor needed only 97 datapoints to create a consistent enough metamodel ( $LOO \simeq 0.0647$ ). This shows great interest of using the quad-tree design coupled with uniform sampling as many datapoints (most of the corners) are within several subdomains, which is not the case for other sampling methods. For instance, reproducing the same  $50 \times 50$  meshgrid without the metamodel predictor would have required 2500 calls of the computational model.

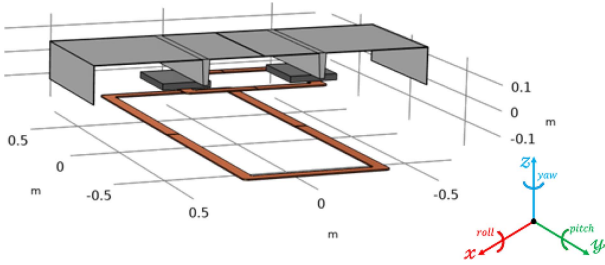


Fig. 8. FEM model for a complete WPT model with 3F3 ferrites cores and an optimized shielding structure.

This brings the crucial need to properly tune the  $LOO$  threshold  $\varepsilon$  and the maximum number of divisions  $m$  of the active learning algorithm regarding the model behavior and its dimensionality. As the performance of this algorithm has been fully validated on classical analytical functions, the goal is to extend its application to heavy computational model such as FEM model, where the gain in computation time could be of great use.

#### IV. APPLICATION TO A REALISTIC WPT SYSTEM MODEL

The goal here has been to apply the metamodeling algorithm on a realistic FEM model for a WPT system developed at the Politecnico di Torino [22]. Based on this complex model, our algorithm tries to build a consistent predictor that can be used for both SA and optimization design in lieu of the real model to save computation time.

##### A. Computational Model

Using the computer-aided design model from the WPT system receiver used for experiments at the Politecnico di Torino, the complete WPT model has been reproduced with a 3-D FEM model displayed in Fig. 8. For the receiving device, only the main shielding structure optimized with the shielding beams, along with the double U-shaped coils (displayed in orange in Fig. 8) topped by the 3F3 ferrite cores, has been considered, while only the transmitting coil in the ground has been modeled for the transmitter.

Because this model is fitting a real model available inside the laboratory, the effects of mostly design-based geometrical parameters have been considered:

- 1)  $\Delta x$ ,  $\Delta y$ , and  $\Delta z$ : the misalignments between the receiving and transmitting coils along the  $x$ -,  $y$ -, and  $z$ -axes;
- 2)  $w_{\text{coil}}$ ,  $l_{\text{coil}}$ ,  $w_{\text{tcoil}}$ ,  $l_{\text{tcoil}}$ : the dimensions of the coils;
- 3)  $\alpha$ ,  $\beta$ ,  $\gamma$ : the yaw, pitch, and roll of the transmitting coil.

The output considered in the following analysis is the coupling factor  $k$  of the WPT system:

$$k = \frac{M}{\sqrt{L_R L_T}} \quad (12)$$

where  $M$  is the mutual inductance of the two coils and  $L_R$  and  $L_T$  are their respective self-inductances.

Regarding the computation time, one datapoint takes  $\sim 1$  min to compute on an Intel Core i7-10610U, 1.80 GHz, 8 GB of

TABLE I  
PARAMETERS WITH THEIR CORRESPONDING RANGES FOR THE ANALYSIS OF A DYNAMIC WPT SYSTEM ( $LOO \simeq 0.030018765223648$ ,  $n_{\text{samples}} = 65$ )

variable	min	max	description	$S^T$
$\Delta x$	-0.25 m	0.25 m	$x$ misalignment	0.139
$\Delta y$	-0.5 m	0.5 m	$y$ misalignment	0.138
$\Delta z$	-0.15 m	0.15 m	$z$ misalignment	0.261
$\alpha$	$-10^\circ$	$10^\circ$	yaw	0.136
$\beta$	$-2^\circ$	$2^\circ$	pitch	$1.97 \cdot 10^{-3}$
$\gamma$	$-2^\circ$	$2^\circ$	roll	0.634

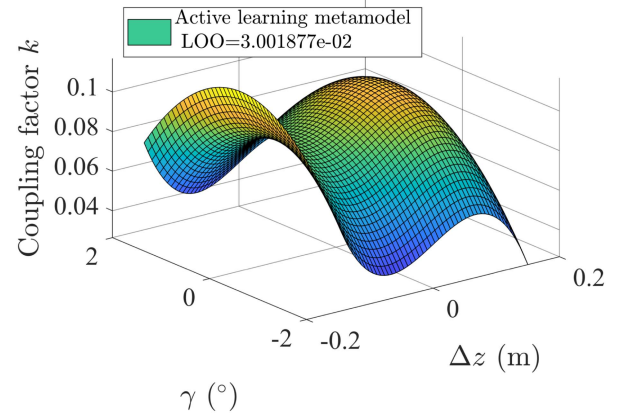


Fig. 9. Variations of the coupling factor  $k$  against the  $z$  misalignment  $\Delta z$  and the roll  $\gamma$  ( $\Delta x = \Delta y = 0$  m and  $\alpha = \beta = 0^\circ$ ).

RAM. If one were to perform some brute-force SA (using MC sampling, for example), this would require a few thousand calls of the computational model. Thus, the total computation time of the analysis would be several days.

##### B. Sensitivity to the Road Profile

The first application has been to compute a consistent predictor for the behavior of the coupling factor regarding the movement of the vehicle and the road profile. The considered parameters for this analysis are displayed in Table I. The  $\Delta x$  misalignment and the yaw  $\alpha$  have been chosen to consider a car slightly deviating from the center of the road, while the  $\Delta y$  misalignment embodies the direction of motion. The  $\Delta z$  misalignment along with the pitch  $\beta$  and the roll  $\gamma$  take into account the road profile.

The active learning metamodel algorithm managed to build a consistent predictor with  $\varepsilon = 0.3$  and  $m = 3$ . The resulting metamodel uses  $n_{\text{samples}} = 65$  and has a consistency of  $LOO \simeq 0.030018765223648$ . An example of the variation of the coupling factor produced by the active learning metamodel predictor is displayed in Fig. 9 for the variations of  $\Delta z$  and  $\gamma$  (a modification of the road profile) with the other parameters set at their nominal values ( $\Delta x = \Delta y = 0$  m and  $\alpha = \beta = 0^\circ$ ).

Using this consistent predictor, an SA has been computed using total Sobol' indices displayed in Table I. The most important parameters are the roll  $\gamma$  along with the  $\Delta z$  misalignment. As expected, these two parameters greatly increase the distance



TABLE II  
PARAMETERS WITH THEIR CORRESPONDING RANGES FOR THE ANALYSIS OF A DYNAMIC WPT SYSTEM ( $LOO \simeq 0.0141$ ,  $n_{\text{samples}} = 17$ )

variable	min	max	description	$S^T$
$w_{\text{coil}}$	0.3 m	0.6 m	receiving coil width	0.105
$l_{\text{coil}}$	0.3 m	0.6 m	receiving coil length	0.177
$w_{\text{coil}}$	0.3 m	0.6 m	transmitting coil width	0.0614
$l_{\text{coil}}$	0.5 m	2 m	transmitting coil length	0.691

TABLE III  
MAXIMUM NUMBER OF DATAPPOINTS  $n_{\text{max}}$  COMPUTED AGAINST THE DIMENSION OF THE INPUT SPACE  $d$  AND THE MAXIMUM NUMBER OF DIVISIONS  $m$

$n_{\text{max}}$	$m = 0$	$m = 1$	$m = 2$	$m = 3$	$m = 4$
$d = 1$	3	5	9	17	33
$d = 2$	5	13	41	145	545
$d = 3$	9	35	189	1 241	9 009
$d = 4$	17	97	881	10 657	149 057
$d = 5$	33	275	4 149	91 817	2 468 433
$d = 6$	65	793	19 721	793 585	40 914 785

between the two coils, which decreases significantly the coupling factor. Even if the pitch  $\beta$  also influences the gap between the receiver and the transmitter, for this small range  $[-2^\circ, 2^\circ]$  corresponding to an imperceptible bump on the road, its effect is entirely negligible. The roll embodies a nonflatten road that has still a greater impact with such a small range. The other three parameters  $\Delta x$ ,  $\Delta y$ , and  $\alpha$  are taking into account the dynamic aspect for the WPT system and are of course not negligible.

### C. Sensitivity to Various Coil Dimensions

Another interesting analysis is to assess the dependence of the coupling factor regarding the transmitter or receiver dimensions. This could emphasize where the greatest care should be taken when designing or building a new WPT system. The considered parameters with their ranges and Sobol' indices are displayed in Table II. The algorithm has been run with  $\varepsilon = 0.3$  and  $m = 3$  resulting in a metamodel with  $LOO \simeq 0.0141$  and  $n_{\text{samples}} = 17$ .

The length of the transmitting coil is by far the most important parameter regarding the coupling factor behavior. It ensures that the totality of the magnetic flux generated is embraced by the receiving coil. Owing to the chosen possible dimensions, for the same reason, the length of the receiver is also extremely important. As the nominal gap between the coils is  $\Delta z = 23.5$  cm, the width of the transmitter has a lesser influence as long as the totality of the magnetic flux can be directed to the receiver, which is ensured with a range [0.3 m, 0.6 m] similar to the maximum dimensions of the receiver. The receiver dimensions are only limited by the car it can be put in and, therefore, cannot be extended.

### D. Discussion on the Algorithm Parameters

In Table III, the dependence of the maximum number of computed datapoints  $n_{\text{max}}$  [see (11)] against the dimension of

TABLE IV  
COMPUTATION TIME OF THE VARIOUS STEPS

Analysis	$n_{\text{samples}}$	computation time of all metamodels	computation FEM model	computation SA
road profile	65	$\sim 1.92$ s	1 h	$\sim 245$ ms
coil dimensions	17	$\sim 1.55$ s	15 min	$\sim 130$ ms

TABLE V  
ESTIMATED GAIN IN COMPUTATION TIME FOR THE STUDIES ON THE WPT CHARGER MODEL

Analysis	$d$	$LOO$	brute-force analysis (estimated)	adaptive metamodeling algorithm	time reduction
road profile	6	0.030	1.5 years	1 h	99.99%
coil dimensions	4	0.014	7 days	15 min	99.85%

the input space  $d$  and the maximum number of divisions  $m$  is displayed for several values. Using the algorithm, if one were to diminish the consistency threshold  $\varepsilon$  to less than 1% for example, the metamodel for the coil dimensions ( $m = 3, d = 4$ ) would need the maximum  $n_{\text{max}} = 10\,657$ , while  $n_{\text{max}} = 793\,585$  for the WPT dynamic analysis ( $m = 3, d = 6$ ). Thus, the computation of a metamodel with a higher local consistency would be almost impossible as one datapoint takes  $\sim 1$  min to compute if the resulting submetamodels are not consistent.

### E. Gain in Computation Time

The goal of the two analyses presented here has been to try our active learning algorithm for accurate SA, in order to save computation time compared to classical methods. When looking at the algorithm flowchart in Fig. 2, the total computation time for a run of the algorithm needs to consider three different contributions: the calls of the expensive computational model, the computation of the metamodels at every loop, and finally the SA.

In Table IV, the total computation time of the various steps of the algorithm is displayed for both the analyses. As expected, the only time-consuming step is the call of the FEM model. The computation time of all the metamodels computed in a single run of the algorithm put together does not exceed 2 s for both the cases, while the two SAs are taking less than 1 s. Therefore, the total computation time of the algorithm can be reduced to the calls of the FEM model.

These computation times have been compared to that of a brute-force analysis where a uniform grid with  $n_{\text{max}}$  samples has been computed [see (11)]. The results are displayed in Table V; the estimated computation time with an extremely refined uniform grid would be in days or even years at six parameters, while our algorithm does not last more than 1 h. Thus, the gain in computation time using this active learning metamodeling algorithm is over 99%. Even if some way better sampling methods (such as MC, LHS, Halton, etc.) could be used in a classical analysis to build the surrogate model, the

time reduction compared to a uniform grid would not be greater than 99% [23].

## V. CONCLUSION

In this article, an adaptive sampling algorithm designed for PCK metamodelling of complex EM problem was successfully developed. Two analyses on a realistic FEM model were performed to show the usefulness of such an algorithm. The two computed metamodels had a great consistency ( $LOO < 3\%$ ), which is sufficient for drawing tendencies for SA. The results can be used for future designs or EMC analysis of WPT systems for automotive applications.

As previously developed, the algorithm could show limitations at high-dimensional input space. An easy solution to this problem is to decrease the number of input parameters by performing factor prioritization. A first wide analysis can be performed on various parameters, giving us a consistent predictor for the model able to perform an accurate SA. Using this SA, only the relevant parameters can be extracted and a finer input space can be chosen with the negligible parameters ignored. Then, a better and more consistent metamodel can be built on this smaller set of parameters as it will be able to fully explore the input parameter space thanks to its smaller dimension.

Many improvements for such a numerical method are still possible, but using this algorithm on various FEM models saved more than 99% of computation time compared to classical brute-force analysis. Thus, this method is of great interest for future SA in the case of complex EM systems.

## REFERENCES

- [1] I. M. Sobol, "Sensitivity analysis for non-linear mathematical models," *Math. Model. Comput. Exp.*, vol. 1, pp. 407–414, 1993.
- [2] B. Iooss and P. Lemaître, "A review on global sensitivity analysis methods," in *Uncertainty Management in Simulation-Optimization of Complex Systems*. New York, NY, USA: Springer, 2015, pp. 101–122.
- [3] Y. Wang, S. Jin, S. Penugonda, J. Chen, and J. Fan, "Variability analysis of crosstalk among differential vias using polynomial-chaos and response surface methods," *IEEE Trans. Electromagn. Compat.*, vol. 59, no. 4, pp. 1368–1378, Apr. 2017.
- [4] K. Patra, S. Cheruvalath, S. Dhar, B. P. Nayak, A. Gupta, and J. Hansen, "Surrogate modeling for predicting shielded cable emissions," *IEEE Trans. Electromagn. Compat.*, vol. 65, no. 1, pp. 249–256, Jan. 2022.
- [5] H. Chen, Y. Zhang, Y. Du, and Q. S. Cheng, "Fast design of multilayered shields using surrogate model and space mapping," *IEEE Trans. Electromagn. Compat.*, vol. 62, no. 3, pp. 698–706, Mar. 2019.
- [6] S. Koziel and A. Pietrenko-Dabrowska, "Knowledge-based performance-driven modeling of antenna structures," *Knowl.-Based Syst.*, vol. 237, 2022, Art. no. 107698.
- [7] P. Li and L. J. Jiang, "Uncertainty quantification for electromagnetic systems using ASGC and DGTD method," *IEEE Trans. Electromagn. Compat.*, vol. 57, no. 4, pp. 754–763, Apr. 2015.
- [8] H. Liu, Y.-S. Ong, and J. Cai, "A survey of adaptive sampling for global metamodelling in support of simulation-based complex engineering design," *Struct. Multidisciplinary Optim.*, vol. 57, no. 1, pp. 393–416, 2018.
- [9] R. Trincherio, I. S. Stievano, and F. G. Canavero, "Black-box modeling of the maximum currents induced in harnesses during automotive radiated immunity tests," *IEEE Trans. Electromagn. Compat.*, vol. 62, no. 2, pp. 627–630, Feb. 2019.
- [10] T. Bdour, C. Guiffaut, and A. Reineix, "Use of adaptive kriging metamodelling in reliability analysis of radiated susceptibility in coaxial shielded cables," *IEEE Trans. Electromagn. Compat.*, vol. 58, no. 1, pp. 95–102, Jan. 2015.
- [11] A. Bingler, S. Bilicz, and M. Csörnyei, "Global sensitivity analysis using a kriging metamodel for em design problems with functional outputs," *IEEE Trans. Magn.*, vol. 58, no. 9, Sep. 2022, Art. no. 7501004.
- [12] L. Lebensztajn, C. A. R. Marretto, M. C. Costa, and J.-L. Coulomb, "Kriging: A useful tool for electromagnetic device optimization," *IEEE Trans. Magn.*, vol. 40, no. 2, pp. 1196–1199, Mar. 2004.
- [13] P. Offermann and K. Hameyer, "A polynomial chaos meta-model for non-linear stochastic magnet variations," *COMPEL—Int. J. Comput. Math. Elect. Electron. Eng.*, vol. 32, pp. 1211–1218, 2013.
- [14] P. Kersaudy, B. Sudret, N. Varsier, O. Picon, and J. Wiart, "A new surrogate modeling technique combining kriging and polynomial chaos expansions—application to uncertainty analysis in computational dosimetry," *J. Comput. Phys.*, vol. 286, pp. 103–117, 2015.
- [15] R. Schobi, B. Sudret, and J. Wiart, "Polynomial-chaos-based kriging," *Int. J. Uncertainty Quantification*, vol. 5, no. 2, pp. 171–193, 2015.
- [16] S. Marelli and B. Sudret, "UQLab: A framework for uncertainty quantification in Matlab," in *Vulnerability, Uncertainty, and Risk: Quantification, Mitigation, and Management*. Reston, VA, USA: ASCE, 2014, pp. 2554–2563.
- [17] P. Jiang, L. Shu, Q. Zhou, H. Zhou, X. Shao, and J. Xu, "A novel sequential exploration-exploitation sampling strategy for global metamodelling," *IFAC-PapersOnLine*, vol. 48, no. 28, pp. 532–537, 2015.
- [18] A. Elisseff and M. Pontil, "Leave-one-out error and stability of learning algorithms with applications," *NATO Sci. Ser., III, Comput. Syst. Sci.*, vol. 190, pp. 111–130, 2003.
- [19] R. A. Finkel and J. L. Bentley, "Quad trees a data structure for retrieval on composite keys," *Acta Informatica*, vol. 4, no. 1, pp. 1–9, 1974.
- [20] T. Braconnier, M. Ferrier, J.-C. Jouhaud, M. Montagnac, and P. Sagaut, "Towards an adaptive POD/SVD surrogate model for aeronautic design," *Comput. Fluids*, vol. 40, no. 1, pp. 195–209, 2011.
- [21] T. J. Mackman, C. B. Allen, M. Ghoreyshi, and K. Badcock, "Comparison of adaptive sampling methods for generation of surrogate aerodynamic models," *AIAA J.*, vol. 51, no. 4, pp. 797–808, 2013.
- [22] V. Cirimele, "Design and integration of a dynamic IPT system for automotive applications," Ph.D. dissertation, Politecnico di Torino, Torino, Italy, 2017. [Online]. Available: <https://www.theses.fr/2017SACLS032>
- [23] C. Kamath, "Intelligent sampling for surrogate modeling, hyperparameter optimization, and data analysis," *Mach. Learn. Appl.*, vol. 9, 2022, Art. no. 100373.